Available online at www.sciencedirect.com

ScienceDirect

Proceedings of the Combustion Institute 39 (2023) 467–476

Proceedings of the Combustion Institute

www.elsevier.com/locate/proci

Identification of homogeneous chemical kinetic regimes of methane-air ignition

Éva Valkó [a,b], Máté Papp [b], Peng Zhang [b], Tamás Turányi [b,*]

[a] *Institute of Mathematics, ELTE Eötvös Loránd University, Budapest, Hungary*
[b] *Institute of Chemistry, ELTE Eötvös Loránd University, Budapest, Hungary*

Received 1 January 2022; accepted 22 July 2022
Available online 15 October 2022

Abstract

Sensitivity analysis results for ignition delay time (IDT) may be very different depending on the initial temperature, pressure and equivalence ratio φ, but similar in some regions of these variables. This phenomenon was investigated systematically by carrying out ignition simulations and local sensitivity calculations of methane−air mixtures using the Aramco-II-2016 mechanism at 14,417 combinations of initial temperature (changed between 500 and 3000 K), initial pressure (0.05−500 atm) and φ (0.05−8.0) values. The cluster analysis of the sensitivity vectors identified five large kinetically homogeneous regions. Each region has well defined borders in the (T, p φ) space and can be characterized by different sets of important reactions. The related kinetic scheme is very different in each region. Regions 1 and 2 are dominated by catalytic cycles based on species CH_3O_2/CH_3O_2H and HO_2/H_2O_2/CH_3O, respectively. In regions 3, 4, and 5 the H atoms are converted to CH_3 in an identical chain branching sequence, but the back conversion is via three different routes. Literature experimental data on the IDTs of methane−air mixtures were sorted according to these five regions. Regions 1 to 5 contain 214, 328, 3, 0, and 237 experimental data points, respectively. In regions 1, 2 and 5 the data points are well reproduced by the Aramco-II-2016 mechanism, but little or no experimental information is available about kinetic regions 3 and 4. Further experimental exploration of the ignition of methane−air mixtures may aim the study of these regions. A similar approach can be used for the characterization of other combustion systems and sorting the related experimental data.

Keywords: Methane ignition; Ignition delay time; Kinetic regimes; Sensitivity analysis

* Corresponding author.
E-mail address: turanyi@chem.elte.hu (T. Turányi).

https://doi.org/10.1016/j.proci.2022.07.186

1. Introduction

The homogeneous ignition of methane–air mixtures starts with [1] initiation reactions

$$CH_4 + M = CH_3 + H + M \quad (R1)$$

$$CH_4 + O_2 = CH_3 + HO_2 \quad (R2)$$

Then, the radicals CH_3, H and HO_2 formed participate in a series of homogeneous catalytic reactions that increase the concentrations of the radicals. There are also other reactions that consume the radicals. When the extent of radicals or radical precursors reaches a critical limit, then sudden ignition occurs.

Frenklach et al. [2] found that the induction period for stoichiometric mixtures is most sensitive to the rates of chain branching processes

$$CH_3 + O_2 = CH_3O + O \quad (R3)$$

$$H + O_2 = OH + O \quad (R4)$$

Sloane [3] emphasized that reactions

$$CH_3 + CH_3 + M = C_2H_6 + M \quad (R5)$$

$$CH_4 + H = CH_3 + H_2 \quad (R6)$$

play an important role by inhibiting the induction process. Sloane also stressed that reaction

$$CH_3 + CH_3 = C_2H_5 + H \quad (R7)$$

is a promoting reaction, which is converting methyl radicals to more reactive H-atoms.

Spadaccini and Colket [4] confirmed that reactions R3 to R7 are important for the control of the radical pool above 1500 K. They found that these reactions are also important below 1500 K:

$$CH_4 + HO_2 = CH_3 + H_2O_2 \quad (R8)$$

$$H_2O_2 + M = 2\,OH + M \quad (R9)$$

$$CH_2O + O_2 = HCO + HO_2 \quad (R10)$$

Metcalfe et al. [5] investigated the most sensitive reactions at methane ignition, confirmed the importance of reactions R4, R5, R6, R8 and R10, and listed the following further important reactions:

$$CH_3 + O_2 = CH_2O + OH \quad (R11)$$

$$CH_3 + HO_2 = CH_3O + OH \quad (R12)$$

$$CH_3O_2 + CH_3 = 2\,CH_3O \quad (R13)$$

$$2\,HO_2 = H_2O_2 + O_2 \quad (R14)$$

$$H + O_2 + M = HO_2 + M \quad (R15)$$

$$CH_3 + HO_2 = CH_4 + O_2 \quad (R16)$$

Here R5, R6, R14, R15 and R16 were identified as ignition inhibiting reactions.

Hashemi et al. [6] discussed the importance of reaction steps in the ignition of methane–air mixtures under intermediate temperature and high pressure conditions. They demonstrated the importance of reactions R2, R4, R5, R8, R11, R12 and R14 under such conditions.

Zhang et al. [7] aimed to collect all published experimental data related to the ignition of methane–oxygen mixtures. The possible other initial components included CO and H_2 as added fuel and N_2, H_2O, CO_2, Ar and He as diluents. Zhang et al. collected 5521 data points in 643 datasets from 76 publications. These experimental data covered the following initial conditions: T: 803–2800 K, p: 0.069–481.4 atm, and φ: 0.03–8.0. All these data can be downloaded from the ReSpecTh data collection [8] in RKD v2.3 data format [9]. Thirteen recent methane combustion mechanisms were tested against these experimental data, and Aramco-II-2016 was identified as the one that most accurately reproduced the experimental data in wide ranges of temperature T, pressure p, equivalence ratio φ, and diluent concentration.

Zhang et al. carried out sensitivity analysis calculations to each experimental data point using several combustion mechanisms. These calculations showed that initial conditions related to some groups of data points provided very similar sensitivity results and these groups could be related to regions of T, p, and φ.

In this work this topic is investigated further in a systematic way. Several thousand initial states of methane–air mixtures were generated on a grid of conditions. The highest and lowest values of T, p, and φ in the grid are approximately equal of those of the available experimental data. Local IDT sensitivity results were calculated to each grid point and the sensitivity vectors were sorted to groups by cluster analysis. The calculations revealed that the methane ignition system can be related to kinetically homogeneous regimes. This paper contains a chemical kinetics discussion of these regimes and investigates the available experimental data for each regime.

2. Details of sensitivity analysis and clustering calculations

The ignition of methane–air mixtures was simulated using the Aramco-II-2016 methane combustion mechanism [10]. The simulations were carried out using the OpenSMOKE++ simulation package [11,12]. Ignition delay time was defined by the maximum of the time derivative of the OH^*

concentration. Adiabatic, constant volume ignition system was simulated. The type of simulations and the IDT definition are in accordance with the simulations of most shock tube experiments (see Table 3 in [7]).

Ignition of methane−air mixtures was investigated on a grid by systematically changing the initial temperature, pressure, and equivalence ratio. Initial temperature was changed from 500 K to 3000 K by step 100 K (26 values). Pressure was changed from 0.05 atm to 500 atm on 20 logarithmically equidistant levels and $p = 1.00$ atm was added (21 values). Equivalence ratio φ was changed from 0.05 to 1 in steps 0.05 and from 1 to 8.0 in steps 0.5 (34 values). The exact values of the grid points are given in Supplementary 1.

The size of the grid is $26 \times 21 \times 34$, therefore these values define 18,564 combinations of initial temperature, initial pressure and φ values. The final simulation time was 10 s and up to this time, ignition was observed in 14,417 cases. For each successful simulation, the following data were recorded: ignition delay time, temperature, pressure and composition at the time of ignition and the local IDT sensitivity vector.

The original full Aramco-II-2016 mechanism (2716 reactions of 502 species) was truncated by eliminating the species having more than two carbon atoms and their reactions. The obtained mechanism can be downloaded from [8]. It is identical to that was used by Zhang et al. [7] for mechanism testing, and contains 490 reactions of 86 species. The normalized local sensitivity coefficients ($\partial \ln\{\tau\}/\partial \ln\{A\}$) of the ignition delay time τ were calculated by the Optima++ framework code [13] using the finite difference approach with 5% perturbation of the Arrhenius A-factors. The A-factors of the low-pressure and high-pressure limits were handled separately, resulting in a sensitivity vector of 519 elements.

In another series of calculations, the ignition delay times and sensitivity vectors were calculated for all experimental data points that belong to methane–air ignition experiments in the ReSpecTh database. These experiments had been carried out in shock tubes and rapid compression machines (RCMs). We considered only experiments, where the fuel was neat methane (without added H_2 or CO), the diluent was N_2 or Ar, and the oxidizer consisted of 19% to 23% O_2. Data flagged as potentially not reliable by Zhang et al. (indicated by grey shading in Table A in the Supplementary of paper [7]) were excluded from the analysis. 1038 data points in 101 data sets remained after the exclusions. The simulations were carried out exactly at the conditions of the experiments, using the Optima++ framework code [13] and the OpenSMOKE++ simulation package [11]. We always fully took into account the facility effects. The details of these simulations and sensitivity calculations have been described in the article of Zhang et al. [7].

The agreement of the simulated (τ_i^{sim}) and experimental (τ_i^{exp}) ignition delay time in measurement i is characterized by the following error function:

$$E_i = \left(\frac{\ln \tau_i^{\text{sim}} - \ln \tau_i^{\text{exp}}}{\sigma\left(\ln \tau_i^{\text{exp}}\right)} \right)^2 \tag{1}$$

The experimental IDT data and their 1σ uncertainty are given in the corresponding ReSpecTh datafiles. The IDs of the datafiles used are listed in Supplementary 2.

The vectors of normalized local sensitivity coefficients were used to calculate the distance that characterizes the chemical kinetic similarity of two simulations. The distance function d for two normalized local sensitivity vectors $\mathbf{x}$ and $\mathbf{y}$ is defined by

$$d(\mathbf{x}, \mathbf{y}) = 1 - \cos\gamma = 1 - \frac{\mathbf{x} \cdot \mathbf{y}}{|\mathbf{x}| \cdot |\mathbf{y}|}, \tag{2}$$

where γ is the angle between $\mathbf{x}$ and $\mathbf{y}$, d is called the cosine distance of the vectors and $|\cdot|$ denotes Euclidian norm. This cosine distance has been used by Zádor et al. [14] in the context of the similarity of the sensitivity vectors.

The grid points were sorted to groups according to the similarity of their sensitivity vectors. The creation of the groups was based on the clustering of the local sensitivity vectors, using the Weighted Pair Group Method with Arithmetic Mean (WPGMAM) algorithm [15]. This is an agglomerative hierarchical clustering method, which means that in every step of the clustering procedure, the closest two points are contracted, till all the points are contracted into a single cluster. To measure the distance between clusters, the algorithm calculates the pairwise distance between the elements of different clusters and takes the average of it. For the determination of the optimal number of clusters, the Gap distance function method [16] was used. This method uses the output of any clustering algorithm, comparing the within-cluster dispersion of the assumed clusters with that expected from a reference null distribution. The clustering calculations were carried out using the Statistics and Machine Learning Toolbox of Matlab [17].

An alternative methodology could be based on the approach of Wang et al. [18]. They determined a similarity coefficient between two kinetic systems by calculating the cosine similarity between the characteristic vectors of the High Dimensional Model Representation (HDMR) models. However, making a surrogate model based on the HDMR decomposition requires much more computer time compared to the calculation of the local IDT sensitivity vector.

The chemical transformations of species are depicted in reaction flux charts in Supplementary 1.

Table 1
The distance of the representative grid points of the 5 clusters from each other.

Gridpoint	1	2	3	4	5
1	0.00	0.77	0.97	0.91	0.92
2		0.00	0.64	0.42	0.41
3			0.00	0.23	0.14
4				0.00	0.15
5					0.00

Revel et al. [19] suggested that the reaction fluxes have to be visualized on the basis of the fluxes of elements from one species to another during the course of a reaction. This concept is discussed in details in Chapter 4 of the book of Turányi and Tomlin [20]. The chemical kinetics features of the reacting mixtures were analyzed by home-made code FluxViewer++ [21]. This code is able to visualize the change of element fluxes in time (or distance in flames) and investigate the main contributions of the reaction steps to the production rates of species (see Fig. S1).

3. Five homogeneous kinetic regimes of the ignition of methane–air mixtures

The cluster analysis identified five clusters of sensitivity vectors and thus sorted all grid points to five groups. A representative grid point was chosen in each cluster in such a way that the average distance d between each point and all other grid points in a cluster was calculated and the grid point with minimal average distance was chosen.

Table 1 shows the distance of the representative points of the clusters from each other. Clusters 1 and 2 are very well separated from each other and also from all the other clusters. Clusters 3 and 4 are also fairly well separated from each other, the distance of the representative points is larger than 0.2. The separation of cluster 5 from clusters 3 and 4 is not so good, the corresponding distances are only 0.14 and 0.15, respectively.

First, the similarity of the vectors was investigated. Fig. S2 in Supplementary 1 shows distance d of each sensitivity vector of a cluster from the sensitivity vector of the representative grid point. In clusters 1 to 3 and 5, most of the vectors are very similar (distance < 0.2) to the sensitivity vector of the representative point. The exception is cluster 4, where only one quarter of the grid points have sensitivity vector that is highly similar to those of the representative point.

The algorithm of clustering results in that all grid points are sorted to one of the clusters. However, the later chemical kinetics reasoning will be based on the assumption that the sensitivity vectors in each cluster are alike. Therefore, we exclude those points from each cluster that are further than $d = 0.2$ from its representative point. The original clusters 1 to 5 contain 824, 3839, 2498, 3410, and 3846 grid points, while the truncated ones contain 698, 2830, 2095, 979, and 3414 grid points, respectively. Although many of the original grid points are now not sorted to any of the clusters, the sensitivity vectors of the remaining ones are much more alike.

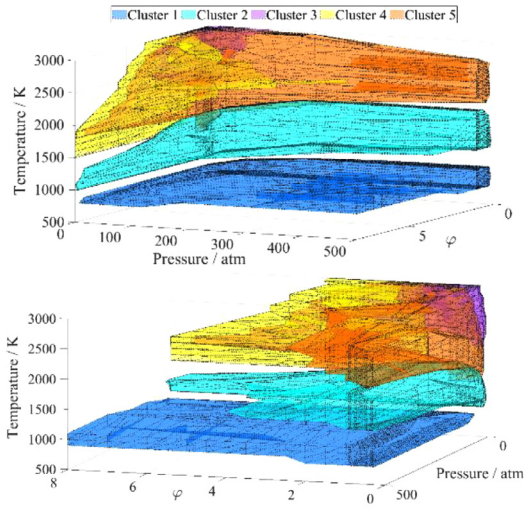

Fig. 1. Location of the regions in the (T, p, φ) space; two different views.

Table 2 shows the main features of the five truncated clusters. From now on term 'cluster' will be used for the truncated clusters. The table contains the minimum and maximum initial T, p and φ values related to the grid points of each cluster.

However, these intervals overlap and therefore the locations of the clusters can be understood from a 3D figure only (see Fig. 1). Supplementary 3 contains a video that gives an even more visual representation of the locations of the clusters.

In the representative points, the normalized IDT sensitivities and the relative net reaction rates at a selected time were calculated. The results are given in Table S1 of Supplementary 1, and its content is summarized in Table 3. In each cell of this table, shading indicates a reaction step with absolute normalized ignition delay time (IDT) sensitivity higher than 0.05. Absolute sensitivities higher than 0.1 are indicated by darker shading. Green and red colours show that increasing the rate coefficient increases or decreases the rate of combustion, i.e. shortens or makes longer the IDT, respectively. Labels HP and LP indicates if the sensitivity coefficient belongs to the A factor of the high- or low-pressure limit rate parameter set, respectively.

Table 2
The main features of the five truncated clusters.

#	colour	grid points	T interval / K	p interval / atm	φ interval	representative grid point			experimental data	
						T_0/K	p_0/atm	φ	number of points	$E_{average}$
1	dark blue	698	800–1100	6.37–500	0.15–8	1000	189.63	1.0	214	1.697
2	light blue	2830	1000–2000	0.05–500	0.05–8	1400	27.3	0.65	328	0.858
3	purple	2095	2000–3000	0.05–116.8	0.05–3.5	2500	0.9	0.35	3	0.302
4	yellow	979	1500–3000	0.05–307.9	1.5–8	2100	1.5	6.0	0	–
5	orange	3414	1400–3000	0.05–500	0.1–7.5	2100	10.3	0.55	237	1.400

Table 3
Reactions having high sensitivity (green/red shading) and high rate (*). The notation details are discussed in the text.

R	reaction	1	2	3	4	5
1	$CH_4+M=CH_3+H+M$ LP			*		
2	$CH_4+O_2=CH_3+HO_2$					
3	$CH_3+O_2=CH_3O+O$					
4	$H+O_2=OH+O$			*	*	*
5	$CH_3+CH_3+M=C_2H_6+M$ LP		*		*	*
6	$CH_4+H=CH_3+H_2$			*	*	*
7	$CH_3+CH_3=C_2H_5+H$				*	
8	$CH_4+HO_2=CH_3+H_2O_2$	*				
9	$H_2O_2+M=2OH+M$ HP	*	*			
10	$CH_2O+O_2=HCO+HO_2$					
11	$CH_3+O_2=CH_2O+OH$		*	*		*
12	$CH_3+HO_2=CH_3O+OH$	*	*			*
13	$CH_3O_2+CH_3=2CH_3O$	*				
14	$2\ HO_2=H_2O_2+O_2$	*				
15	$H+O_2+M=HO_2+M$ LP	*				
16	$CH_3+HO_2=CH_4+O_2$					
17	$CH_4+CH_3O_2=CH_3+CH_3O_2H$					
18	$H_2O_2+M=2OH+M$ LP					
19	$CH_2O+CH_3O_2=HCO+CH_3O_2H$					
20	$CH_2O+HO_2=HCO+H_2O_2$					
21	$CH_4+OH=CH_3+H_2O$	*	*	*	*	*
22	$CH_3O_2+HO_2=CH_3O_2H+O_2$	*				
23	$HCO+M=H+CO+M$ HP			*	*	*
24	$CH_3+OH=CH_2OH+H$			*		
25	$C_2H_4+H=C_2H_3+H_2$					
26	$CH_3+O_2+M=CH_3O_2+M$ LP	*				
27	$CH_3O+O_2=CH_2O+HO_2$	*	*	*		*
28	$CH_3O_2H=CH_3O+OH$	*				
29	$CH_3O+M=CH_2O+H+M$ LP	*	*			
30	$HCO+O_2=CO+HO_2$	*	*			*
31	$CH_2O+CH_3=HCO+CH_4$		*		*	*
32	$CH_4+O=CH_3+OH$		*	*		*
33	$CH_3+O=CH_2O+H$			*		*
34	$CH_2OH+O_2=CH_2O+HO_2$			*		
35	$C_2H_5+M=C_2H_4+H+M$ LP				*	*
36	$CH_2O+OH=HCO+H_2O$					
37	$CH_2O+H=HCO+H_2$					
38	$H+HO_2=2OH$					
39	$C_2H_6+O=C_2H_5+OH$					
40	$CO+OH=CO_2+H$					
41	$CH_2O+O_2=HCO+HO_2$					
42	$C_2H_3+M=C_2H_2+H+M$ LP					

Star (*) indicates that the rate of the reaction step is at least 10% of the fastest net reaction step at half time of the IDT in the corresponding representative point. Reactions R36−R42 are important at the time of ignition only.

Fig. S3 in Supplementary 1 shows the main H-atom fluxes at reaction time half of the IDT using the initial conditions of the representative points 1 to 5.

In regions 1 to 3, reaction R2 is the single important chain initiation step, and both initiation step R1 and R2 are important in regions 4 and 5.

Fig. S4 provides the concentration−time profiles of selected species and Fig. S5 gives the temperature and OH* concentration profiles enlarged. A feature of the methane ignition processes is the accumulation of secondary fuels and reservoir species in the induction phase. These are CH_2O and H_2O_2 in region 1; CH_2O and C_2H_6 in region 2; C_2H_4 in region 4; and CH_2O in region 5.

The clusters contain grid points that have similar sensitivity vectors, thus the same reactions are important in each grid point. Therefore, a region in the T-p-φ space belonging to a cluster can be characterized by a homogeneous chemical kinetics regime. In the next sections the locations and features of these regions will be discussed.

3.1. *Chemical kinetic regime 1 CH_3O_2 / CH_3O_2H catalytic cycle (low T, middle p, any φ)*

Fig. 1 shows that the corresponding dark blue region is located at low temperatures (800–1100 K), middle range of pressure (10 to 150 atm) and all φ values.

The CH_3 radical generated in initiation step R2 is converted to CH_3O_2 in reaction 26, which is then amplified in the following reaction sequence:

$$CH_4 + CH_3O_2 = CH_3 + CH_3O_2H \quad \text{(R17)}$$

$$CH_3O_2H = CH_3O + OH \quad \text{(R28)}$$

$$CH_3O + M = CH_2O + H + M \quad \text{(R29)}$$

$$CH_4 + OH = CH_3 + H_2O \quad \text{(R21)}$$

$$CH_3 + O_2 + M = CH_3O_2 + M \quad \text{(R26)}$$

$$H + O_2 + M = HO_2 + M \quad (R15)$$

These reactions can be summed up as

$$CH_3O_2 + 2\ O_2 + 2\ CH_4 = CH_2O + HO_2 + 2\ CH_3O_2 + H_2O$$

A by-product of the reaction sequence is CH_2O, which has a continuously increasing concentration and becomes a secondary fuel.

There is also another CH_2O production route from radical CH_3O_2:

$$CH_3O_2 + CH_3 = 2\ CH_3O \quad (R13)$$

$$CH_3 + HO_2 = CH_3O + OH \quad (R12)$$

$$CH_3O + O_2 = CH_2O + HO_2 \quad (R27)$$

A part of radicals CH_3O_2 are converted to molecule CH_3O_2H:

$$CH_3O_2 + HO_2 = CH_3O_2H + O_2 \quad (R22)$$

Reservoir species H_2O_2 is produced mainly in reactions:

$$CH_4 + HO_2 = CH_3 + H_2O_2 \quad (R8)$$

$$2\ HO_2 = H_2O_2 + O_2 \quad (R14)$$

However, a part of H_2O_2 is decomposed in reaction

$$H_2O_2 + M = 2\ OH + M \quad (R9)$$

At the ignition, the accumulated species CH_2O and H_2O_2 are quickly consumed and generate small radicals via reaction steps:

$$H_2O_2 + M = 2\ OH + M \quad (R9)$$

$$CH_2O + OH = HCO + H_2O \quad (R36)$$

$$CH_2O + CH_3 = HCO + CH_4 \quad (R31)$$

$$CH_2O + H = HCO + H_2 \quad (R37)$$

$$CH_2O + O_2 = HCO + HO_2 \quad (R10)$$

$$CH_2O + HO_2 = HCO + H_2O_2 \quad (R20)$$

and then radicals HCO and HO_2 are converted to H and OH in reactions

$$HCO + M = H + CO + M \quad (R23)$$

$$HCO + O_2 = CO + HO_2 \quad (R30)$$

$$H + HO_2 = 2\ OH \quad (R38)$$

Unlike in the other kinetic regimes, R4 is not an important chain branching reaction here and the main inhibition step is the removal of HO_2 in reaction R14.

3.2. Chemical kinetic regime 2 HO_2 / H_2O_2 / CH_3O catalytic cycle (middle T, any p, any φ)

This region is indicated by light blue in Fig. 1 and it is located in the middle temperature range above region 1, in a wide range of pressure and φ values.

The chemical processes in this region can be interpreted by two reaction series, denoted by processes A and B.

Process A is a chain branching sequence that produces CH_3 from HO_2:

$$CH_4 + HO_2 = CH_3 + H_2O_2 \quad (R8)$$

$$H_2O_2 + M = 2\ OH + M \quad (R9)$$

$$CH_4 + OH = CH_3 + H_2O \quad (R21)$$

These reactions together give a subtotal reaction

$$3\ CH_4 + HO_2 = 3\ CH_3 + 2\ H_2O$$

The generated CH_3 radicals produce secondary fuel C_2H_6.

$$CH_3 + CH_3 + M = C_2H_6 + M \quad (R5)$$

Process B converts the CH_3 radicals back to HO_2:

$$CH_3 + O_2 = CH_3O + O \quad (R3)$$

$$CH_3O + O_2 = CH_2O + HO_2 \quad (R27)$$

Process B is also a chain branching process that produces secondary fuel CH_2O in subtotal reaction

$$CH_3 + 2\ O_2 = CH_2O + O + HO_2.$$

Other important reactions in this region:

$$CH_3 + O_2 = CH_2O + OH \quad (R11)$$

$$CH_3 + HO_2 = CH_3O + OH \quad (R12)$$

Temperature is continuously increasing in the induction phase, moving the system to the high temperature combustion state, where R4 becomes the main chain branching reaction. At the ignition, the following reactions become important:

$$H + O_2 = OH + O \quad (R4)$$

$$CH_4 + O = CH_3 + OH \quad (R32)$$

$$CO + OH = CO_2 + H \quad (R40)$$

The generated H, OH, and O radicals quickly eliminate secondary fuels CH_2O and C_2H_6.

3.3. Chemical kinetic regime 3
H/OH/O + CH_2O/HCO catalytic cycles (high T, low p, lean to moderately rich φ)

Region 3 is a small one located in a well-defined corner of the (*T, p, φ*) space, characterized by high temperature, low pressure and lean to moderately rich equivalence ratio. This region is denoted by purple colour in Fig. 1.

During the induction period, the thermal decomposition of CH_4 continuously produces radicals:

$$CH_4 + M = CH_3 + H + M \quad (R1)$$

The main catalytic cycle (Process C) consists of reactions

$$H + O_2 = OH + O \quad (R4)$$

$$CH_4 + O = CH_3 + OH \quad (R32)$$

$$CH_4 + OH = CH_3 + H_2O, \quad (R21)$$

giving a subtotal reaction $H + O_2 + 3\ CH_4 = 3\ CH_3 + 2\ H_2O$.

There is also an alternative, but not chain branching route for H to CH_3 conversion:

$$CH_4 + H = CH_3 + H_2 \quad (R6)$$

The lack of amplification results in a large negative ignition delay time sensitivity for reaction R6.

The generated CH_3 radicals are converted back to H atoms (Process D) via reactions

$$CH_3 + O = CH_2O + H \quad (R33)$$

$$CH_3 + O_2 = CH_2O + OH \quad (R11)$$

$$CH_2O + O_2 = HCO + HO_2 \quad (R10)$$

$$HCO + M = H + CO + M \quad (R23)$$

These conversion routes do not produce a secondary fuel.

At the ignition, the following reactions become important:

$$H + O_2 = OH + O \quad (R4)$$

$$CH_3 + O = CH_2O + H \quad (R33)$$

$$CH_2O + O_2 = HCO + HO_2 \quad (R41)$$

$$HCO + M = H + CO + M \quad (R23)$$

Near the ignition, there is only a moderate increase of temperature, but a strong peak of OH^*.

3.4. Chemical kinetic regime 4
H/OH/O + C_2H_5 catalytic cycles (high T, low to moderate p, rich φ)

Region 4 forms a wedge in the (*T, p, φ*) space, indicated by yellow colour in Fig. 1 and it is mainly surrounded by region 5.

Similarly to region 3, the main catalytic cycle consists of reaction steps R4, R32 and R21, which convert H atoms to CH_3 radicals in a chain branching sequence (Process C). Again, reaction R6 provides a non-amplification bypass route, and therefore this reaction has a large negative IDT sensitivity coefficient.

The difference between regions 3 and 4 is that here the generated CH_3 radicals are converted back to H atoms in Process E via reactions

$$CH_3 + CH_3 = C_2H_5 + H \quad (R7)$$

$$C_2H_5 + M = C_2H_4 + H + M \quad (R35)$$

During these reactions secondary fuels C_2H_4 is accumulated.

At the ignition, the following reactions become important:

$$H + O_2 = OH + O \quad (R4)$$

$$CH_3 + CH_3 + M = C_2H_6 + M \quad (R5)$$

$$C_2H_6 + O = C_2H_5 + OH \quad (R39)$$

$$C_2H_5 + M = C_2H_4 + H + M \quad (R35)$$

$$C_2H_4 + H = C_2H_3 + H_2 \quad (R25)$$

$$C_2H_3 + M = C_2H_2 + H + M \quad (R42)$$

At the ignition the temperature increase is negligible, but ignition time can be determined from the inflection point of the OH^* profile (see Fig. S5).

3.5. Chemical kinetic regime 5
H/OH/O + C_2H_5/OH catalytic cycles (high T wide domain of correlated p and φ values)

This region is mainly located around region 4 in the (T, p, *φ*) space and it is indicated by orange colour in Fig. 1. For the H to CH_3 transformation, the chain branching route (Process C, reactions R4, R32, R21) and the non-branching, chain continuation alternative route (reaction R6) are identical to those of regions 3 and 4.

The difference between this region and regions 3 and 4 is that here there is a yet another route (Process F) for the conversion of the generated CH_3 radicals back to H:

$$CH_3 + CH_3 = C_2H_5 + H \quad (R7)$$

$$C_2H_5 + M = C_2H_4 + H + M \quad \text{(R35)}$$

$$CH_3 + O = CH_2O + H \quad \text{(R33)}$$

$$CH_3 + O_2 = CH_2O + OH \quad \text{(R11)}$$

$$CH_3 + OH = CH_2OH + H \quad \text{(R24)}$$

During this reaction sequence secondary fuels CH_3 and CH_2O are accumulated.

At the ignition, the following reactions become important:

$$H + O_2 = OH + O \quad \text{(R4)}$$

$$CH_3 + O = CH_2O + H \quad \text{(R33)}$$

$$CH_2O + H = HCO + H_2 \quad \text{(R37)}$$

$$HCO + M = H + CO + M \quad \text{(R23)}$$

$$CO + OH = CO_2 + H \quad \text{(R40)}$$

The typical concentrations profiles in this region (see Fig. S4) are very different compared to region 4. Species CH_2O accumulate until ignition and then suddenly decompose resulting in radicals.

4. Available methane–air experimental data for the five kinetic regimes

As it has been detailed in Section 2, we selected 1038 experimental data points in 101 datasets that are related to methane–air ignition shock tube and RCM experiments. For each experimental datapoint the distance from the grid points of each original cluster was calculated and averaged. The datapoint was assigned to the cluster with the lowest average distance. This resulted in the assignment of 375, 377, 8, 0, and 278 data points to original clusters 1 to 5, respectively.

Next, the experimental data points were related to the truncated clusters. A data point belongs to truncated cluster n, if it had been assigned to cluster n in the previous step and its distance is less than $d = 0.2$ from the representative point of cluster n. As a result, the sensitivity vectors of the related data points are all very similar to those of the representative points. This approach resulted in the assignment of 214, 328, 3, 0, and 237 data points to truncated clusters 1 to 5, respectively.

Fig. S6, column A of Supplementary 1 shows error E of the reproduction of the experimental data points as a function of distance d of the datapoint from the representative grid point in the cluster. The E values are low near the representative point, and E is typically higher near distance $d = 0.1$. However, further away from the representative points the error does not increase.

Then, the error function values E of the data points were plotted as a function of ignition temperature, pressure and φ (see Fig. S6, columns B to D). The error function values are higher in temperature regions 2150–2300 K, 2000–2500 K, 2050–2150 K for regions 1, 2 and 5, respectively. The error function values are lower outside these regions. The same reaction steps are important within each truncated cluster at all temperatures, therefore the systematic deviations can be attributed either to experimental difficulties or not well known rate coefficients in these temperature intervals. Considering the effect of pressure, the E values are lower at higher pressures. No systematic change with the value of φ was found in any of the clusters.

The average E values are 1.697, 0.858, and 1.400 in clusters 1, 2, and 5, respectively. A near unity E value means that the model very well reproduces the experimental data.

5. Conclusion

Investigation of combustion systems is usually carried out in such a way that features of the system (like ignition delay time, laminar burning velocity, species profiles) are measured under a wide range of conditions; and initial temperature, pressure, and equivalence ratio are systematically varied. However, it is not obvious how to select these conditions for a comprehensive study. Sometimes a slight shift of temperature or φ switches the system to a chemically qualitatively different state, while in other cases quite large change of the experimental conditions results in an almost identical system from a chemical kinetics point of view.

In this work the starting point of reasoning is that the chemical kinetic features of ignition can be characterized by the local sensitivity vector of the ignition delay time with respect to the A-factors of the detailed reaction mechanism used for the simulation. It is assumed that the similarity of two chemical kinetic regimes related to the conditions of two experiments can be characterized by the distance d of the two sensitivity vectors. This approach has several consequences.

(i) If distance d between two measurements is small, then the two measurements provide similar chemical kinetics information about the system.
(ii) If two measurements are carried out at similar temperatures and pressures, and their distance d is small, then the two measurements should be reproduced with similar accuracy with the same mechanism. If the accuracy of reproduction is very different, then one of the measurements is wrong.
(iii) Definition of a distance between two sensitivity vectors can be used as a basis for the clustering of sensitivity vectors, which means

the clustering of the measurement conditions where these sensitivity vectors had been calculated. This allows the identification of homogenous chemical kinetic regimes of a combustion system. Homogeneous kinetic regime means that the same reactions control ignition in the corresponding domain of measurements conditions, like initial temperature, pressure, and equivalence ratio.

(iv) The approach could be developed into a model-based design of experiments method. Large number of trial conditions within the range of applicability of a laboratory facility can be generated, and the ones are selected as measurement points that are expected to give very different information about the investigated chemical system based on the similarity of the sensitivity vectors. Also, this approach allows the experimentalist to select conditions from the chemically similar ones where measurements are easier to carry out and the results are more accurate.

The concept above was applied for the investigation of the methane−air combustion system. Ignition delay times and sensitivity vectors of ignition delay time were calculated using the Aramco-II-2016 mechanism at 14,417 combinations of initial temperature (changed between 500 and 3000 K), initial pressure (0.05−500 atm) and φ (0.05−8.0) values on a grid. The selection of the mechanism is arbitrary, any other realistic mechanism would have been applicable.

Cluster analysis revealed that in the methane−air ignition system there are five large kinetically homogeneous regimes. These regimes are related to well defined regions, i.e. domains of the (T, p, φ) space. Regime 1 belongs to low temperature and here the chain branching reactions involve species CH_3O_2 and CH_3O_2H. Regime 2 is at mid temperatures and the catalytic cycle includes species HO_2, H_2O_2, and CH_3O. Regimes 3, 4, and 5 all belong to high temperature. In these regimes the H atoms are converted to CH_3 in an identical chain branching sequence, but the CH_3 to H back conversion is via three different routes, which involve species CH_2O/HCO, C_2H_5 and C_2H_5/OH, respectively.

The available experimental data for the methane−air ignition system are sorted according to these five clusters. Much experimental data are available for clusters 1, 2, and 5, while very little experimental data can be related to clusters 3 and 4. This means that a deeper understanding of the methane−air ignition system could be achieved by doing further measurements at the conditions of clusters 3 (high T, low p, lean to moderately rich φ) and 4 (high T, low to moderate p, rich φ).

Declaration of Competing Interest

The authors declare that they have no known competing financial interests or personal relationships that could have appeared to influence the work reported in this paper.

Acknowledgments

"Application Domain Specific Highly Reliable IT Solutions" project has been implemented with the support provided from the National Research, Development and Innovation Fund of Hungary, financed under the Thematic Excellence Programme TKP2020-NKA-06 (National Challenges Subprogramme) funding scheme. The authors acknowledge the support of NKFIH grant OTKA K132109 of the Hungarian National Research, Development and Innovation Office.

Supplementary materials

Supplementary material associated with this article can be found, in the online version, at doi:10.1016/j.proci.2022.07.186.

References

[1] I. Glassman, R.A. Yetter, N.G. Glumac, Combustion, 5th ed., Academic press, 2014.
[2] M. Frenklach, H. Wang, M.J. Rabinowitz, Optimization and analysis of large chemical kinetic mechanisms using the solution mapping method—combustion of methane, Prog. Energy Combust. Sci. 18 (1992) 47–73.
[3] T.M. Sloane, Ignition and flame propagation modeling with an improved methane oxidation mechanism, Combust. Sci. Technol. 63 (1989) 287–313.
[4] L.J. Spadaccini, M.B. Colket, Ignition delay characteristics of methane fuels, Prog. Energy Combust. Sci. 20 (1994) 431–460.
[5] W.K. Metcalfe, S.M. Burke, S.S. Ahmed, H.J. Curran, A hierarchical and comparative kinetic modeling study of C1 − C2 hydrocarbon and oxygenated fuels, Int. J. Chem. Kinet. 45 (2013) 638–675.
[6] H. Hashemi, J.M. Christensen, S. Gersen, H. Levinsky, S.J. Klippenstein, P. Glarborg, High-pressure oxidation of methane, Combust. Flame 172 (2016) 349–364.
[7] P. Zhang, I.Gy. Zsély, V. Samu, T. Nagy, T. Turányi, Comparison of methane combustion mechanisms using shock tube and rapid compression machine ignition delay time measurements, Energy Fuels 35 (2021) 12329–12351.
[8] ReSpecTh Information System, http://respecth.hu (2022).
[9] T. Varga, C. Olm, M. Papp, Á. Busai, I.G. Zsély, ReSpecTh Kinetics Data Format Specification v2.3 (2020), http://www.respecth.hu
[10] NUI galway combustion chemistry centre AramcoMech 2.0 (2017), http://www.nuigalway.ie/

combustionchemistrycentre/mechanismdownloads/aramcomech20/
[11] OpenSMOKE++, https://www.opensmokepp.polimi.it/, (2022).
[12] A. Cuoci, A. Frassoldati, T. Faravelli, E. Ranzi, OpenSMOKE++: an object-oriented framework for the numerical modeling of reactive systems with detailed kinetic mechanisms, Comput. Phys. Commun. 192 (2015) 237–264.
[13] M. Papp, T. Varga, Á. Busai, I.G. Zsély, T. Nagy, T. Turányi, Optima++ package v2.1.0: a general C++ framework for performing combustion simulations and mechanism optimization, 2021.
[14] J. Zádor, I.G Zsély, T. Turányi, Investigation of the correlation of sensitivity vectors of hydrogen combustion models, Int. J. Chem. Kinet. 36 (2004) 238–252.
[15] M. Sokal, A statistical method for evaluating systematic relationships, Univ. Kans. Sci. Bull. 38 (1958) 1409–1438.
[16] R. Tibshirani, G. Walther, T. Hastie, Estimating the number of clusters in a data set via the gap statistic, J. R. Stat. Soc. Ser. B Stat. Methodol. 63 (2001) 411–423.
[17] Inc. The MathWorks, MATLAB R2020a and Statistics and Machine Learning Toolbox R2021b (2022).
[18] J. Wang, S. Li, B. Yang, Combustion kinetic model development using surrogate model similarity method, Combust. Theory Model. 22 (2018) 777–794.
[19] J. Revel, J.C. Boettner, M. Cathonnet, J.S. Bachman, Derivation of a global chemical kinetic mechanism for methane ignition and combustion, J. Chim. Phys. 91 (1994) 365–382.
[20] T. Turányi, A.S. Tomlin, Reaction pathway analysis, in: Analysis of Kinetic Reaction Mechanisms, Springer, Berlin, Heidelberg, 2014, pp. 53–60.
[21] M. Papp, FluxViewer++, respecth.hu, (2021).